Ann. Geophys., 25, 2007–2017, 2007
www.ann-geophys.net/25/2007/2007/
© European Geosciences Union 2007

Annales Geophysicae

The combined effects of electrojet strength and the geomagnetic activity (K_p-index) on the post sunset height rise of the F-layer and its role in the generation of ESF during high and low solar activity periods

S. Tulasi Ram[1], P. V. S. Rama Rao[1], D. S. V. V. D. Prasad[1], K. Niranjan[1], A. Raja Babu[1], R. Sridharan[2], C. V. Devasia[2], and Sudha Ravindran[2]

[1]Space Physics Laboratories, Department of Physics, Andhra University, Visakhapatnam, India
[2]Space Physics Laboratory, VSSC, Trivandrum, India

Received: 31 March 2007 – Revised: 4 September 2007 – Accepted: 14 September 2007 – Published: 2 October 2007

Abstract. Several investigations have been carried out to identify the factors that are responsible for the day-to-day variability in the occurrence of equatorial spread-F (ESF). But the precise forecasting of ESF on a day-to-day basis is still far from reality. The nonlinear development and the sustenance of ESF/plasma bubbles is decided by the background ionospheric conditions, such as the base height of the F-layer ($h'F$), the electron density gradient (dN/dz), maximum ionization density ($N_{\max}$), geomagnetic activity and the neutral dynamics. There is increasing evidence in the literature during the recent past that shows a well developed Equatorial Ionization Anomaly (EIA) during the afternoon hours contributes significantly to the initiation of ESF during the post-sunset hours. Also, there exists a good correlation between the Equatorial Ionization Anomaly (EIA) and the Integrated Equatorial ElectroJet (IEEJ) strength, as the driving force for both is the same, namely, the zonal electric field at the equator.

In this paper, we present a linear relationship that exists between the daytime integrated equatorial electrojet (IEEJ) strength and the maximum elevated height of the F-layer during post-sunset hours (denoted as peak $h'F$). An inverse relationship that exists between the 6-h average K_p-index prior to the local sunset and the peak $h'F$ of the F-layer is also presented. A systematic study on the combined effects of the IEEJ and the average K_p-index on the post-sunset, peak height of the F-layer (peak $h'F$), which controls the development of ESF/plasma bubbles, is carried out using the ionosonde data from an equatorial station, Trivandrum (8.47° N, 76.91° E, dip.lat. 0.5° N), an off-equatorial station, SHAR (13.6° N, 79.8° E, dip.lat. 10.8° N) and VHF scintillations (244 MHz) observed over a nearby low-latitude station, Waltair (17.7° N, 83.3° E, dip.lat. 20° N). From this study, it has been found that the threshold base height of the F-layer at the equator for the development of plasma bubbles is reduced from 405 km to 317 km as the solar activity decreases from March 2001 (mean Rz=113.5) to March 2005 (mean Rz=24.5). This decrease in threshold height with the decreasing solar activity is explained on the basis of changes in the local linear growth rate of the collisional Rayleigh-Taylor instability, due to the variability of various terms such as inverse density gradient scale length (L^{-1}), ion-neutral collision frequency (ν_{in}) and recombination rate (R) with the changes in the solar activity.

Keywords. Ionosphere (Electric fields and currents; Equatorial ionosphere; Ionospheric irregularities)

Correspondence to: P. V. S. Rama Rao
(palurirao@yahoo.com)

1 Introduction

The equatorial and low-latitude ionosphere is the region where the most important post-sunset electrodynamics play a great role towards the generation of a wide spectrum of plasma density irregularities, generally referred to as equatorial spread-F (ESF). Since Dungey (1956) first proposed the gravitational Rayleigh-Taylor (R-T) instability as the main driving mechanism which triggers the ESF, many linear and nonlinear theories for the R-T instability were developed to simulate the generation of ESF (Balsley et al., 1972; Haerendel, 1973; Ossakow et al., 1979; Kelley, 1989; Sultan, 1996). The general morphological features, such as the variability of ESF with local time, season, geographical location, solar activity and geomagnetic activity conditions, have been extensively reported by several researchers (Chandra and Rastogi,

Published by Copernicus Publications on behalf of the European Geosciences Union.

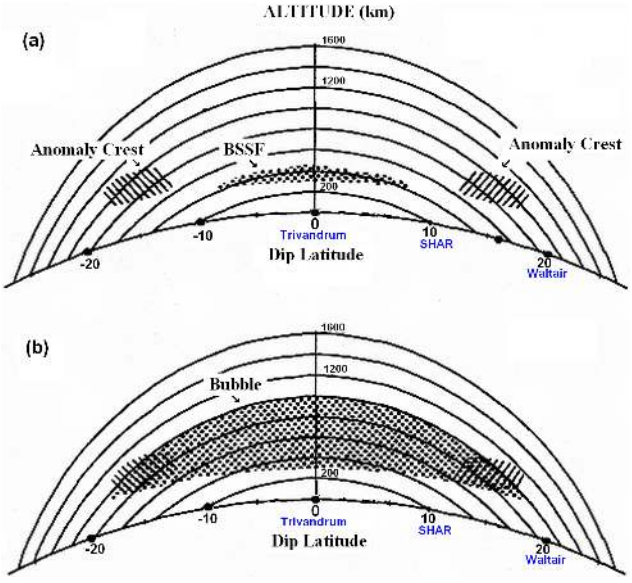

Fig. 1. Illustration showing the distinction between bottom side spread-F (BSSF) and the plasma bubbles as a function of latitude and the geomagnetic field. **(a)** BSSF (shown with dot pattern) is confined to below the F layer maximum and extends along the magnetic field lines to a narrow belt in latitude detectable only by the ionospheric sounders near the dip equator (Trivandrum and/or SHAR). **(b)** An equatorial plasma bubble that rises to high altitude and extends along the magnetic field lines to higher latitudes, detected by all three sounders (Trivandrum, SHAR and Waltair) (after Whalen, 2002).

1972; Woodman and LaHoz, 1976; Sastri et al., 1979; Fejer and Kelley, 1980; Abdu et al., 1981; Aarons, 1993; Fejer et al, 1999; Hysell and Burcham, 2002). However, the accurate forecasting of ESF on a day-to-day basis, which is an essential requirement for satellite-based communication and navigational systems, is still far from reality, owing to the enigmatic day-to-day randomness in their occurrence.

The association of the rapid post-sunset rise of the equatorial F-layer with the occurrence of spread-F was first suggested by Booker and Wells (1938). Several earlier studies have also shown that a rise in the height of the nighttime F-layer is the most important parameter controlling the generation of spread- F (Farley et al., 1970; Ossakow et al., 1979; Rastogi, 1980; Sastri, 1984; Kelley and Maruyama, 1992; Devasia et al., 2002; Jyoti et al., 2004). Further, Fejer et al. (1999), Anderson et al. (2004) and Tulasi Ram et al. (2006) have shown that, when the post-sunset vertical drifts at the equator are large enough, the necessary condition to trigger the ESF always appears to be present.

It is known that both equatorial plasma bubbles and bottom side spread-F (BSSF) are generated after sunset at the bottom side of the F-layer near the dip equator. Although both of these features are described as equatorial spread-F (ESF), these two phenomena have distinct temporal and spatial properties (Woodman and LaHoz, 1976; DasGupta et al., 1983; Argo and Kelley, 1986; Whalen, 1997; Fejer et al., 1999 and Whalen, 2000, 2002). Hysell and Burcham (1998) and Hysell (2000) have explained the differences between bottom-type spread-F, bottom-side spread-F and topside spread-F. The bottom side irregularities develop below the F-region peak with larger primary wavelengths. These bottom side irregularities predominantly drift eastward under the F-region dynamo action and often give rise to ascending depletions that may penetrate to topside ionosphere. The conceptual structure illustrating the distinction between the bottom side spread-F (BSSF) and the plasma bubbles in altitude and latitude is schematically represented in Fig. 1 in a north-south cross section, together with the geomagnetic field lines. This original figure is adopted from Whalen (2002) with a few modifications made to represent the Indian equatorial and low latitude stations.

The bottom side spread-F (BSSF) consists of irregularities that are confined below the peak of the F-layer so as to form a thin layer in altitude (Fig. 1a). As a result, BSSF maps via the magnetic field lines to a narrow belt of latitudes (Aarons, 1993), which is observable only by the sounders located near the dip equator. On the other hand, the bubbles are the plasma depletions and accompanying plumes of irregularities that rise in altitude and extend to a wide band in latitude, which can be detected by the sounders located at latitudes off the dip equator through anomaly crest regions and beyond. The particular importance of plasma bubbles is that, when they extend to the latitudes of the anomaly crest, they intersect with the highest levels of ambient electron density, so that the trans-ionospheric radio-wave propagation through this intersection undergoes high disruptive levels of scintillations, both in amplitude and in phase, with increasing levels during the solar maximum. Fejer et al. (1999) and Whalen (2000, 2002) have shown that the presence of BSSF over the equatorial latitudes is the prerequisite for the development of plasma bubbles. Once the BSSF is present, the nonlinear development of plasma bubbles will be decided by the magnitude of the post-sunset vertical drifts or the maximum height of the F-layer over the equator (Fejer et al., 1999; Whalen, 2002) and also the prevailing background ionospheric conditions, such as the electron density gradient (dN/dz), maximum ionization density ($N_{\max}$), ion-neutral collision frequency (ν_{in}), geomagnetic activity and the neutral winds.

Earlier studies by Raghavarao et al. (1988a); Sridharan et al. (1994); Rama Rao et al. (1997) and Thampi et al. (2006) have shown that the well developed Equatorial Ionization Anomaly (EIA) during the afternoon hours contributes significantly to the initiation of ESF during the post-sunset hours. Also, it has been shown by Raghavarao et al. (1988b), and Rama Rao et al. (2006) that there exists a one-to-one correlation between the Equatorial Ionization Anomaly (EIA) and the Integrated Equatorial ElectroJet (IEEJ) strength, as the driving force for both is the same, namely, the zonal electric field at the equator. Further, Sastri (1998) has shown that

the abnormally large post-sunset height rise of the equatorial F-layer followed by intense spread-F is due to the enhanced daytime EEJ strength, even during the low solar activity periods.

Fejer et al. (1999) have shown that the post-sunset vertical drifts at the equator decreases significantly during the geomagnetically disturbed periods. Later, Whalen et al. (2002), Lee et al. (2005) and Tulasi Ram et al. (2006) have shown that the pre-reversal enhancement in the $\boldsymbol{E}\times\boldsymbol{B}$ drifts decreases linearly with increasing magnetic activity, as measured by a 6-h average K_p-index prior to the local sunset during both high and low solar activity periods. The disturbance dynamo (westward) electric fields associated with enhanced geomagnetic activity (high 6-h average K_p-Index) cause large reductions in the post-sunset vertical drifts. It has also been shown by Whalen et al. (2002), Lee et al. (2005) and Tulasi Ram et al. (2006), that the decrease in post-sunset vertical drifts with increasing average K_p-Index is prominent during equinoxes and winter solstices. Further, Becker-Guedes et al. (2004), from their case studies on the ESF occurrence/suppression during geomagnetic storms over the Brazilian sector, have shown that the enhanced geomagnetic activity acts as an inhibitor during the high spread-F season and acts as an initiator during low spread-F season, possibly due to the corresponding changes in the quiet and disturbed drift patterns during the different seasons.

These results suggest that the daytime EEJ strength contributes positively for the post-sunset height rise of the equatorial F-layer thereby creating conditions favorable for the development of ESF, while the average K_p-index acts as a suppressant for the post-sunset height rise of the equatorial F-layer during equinoxes and winter solstices. Hence, it is reasonable to expect that the daytime Integrated Equatorial ElectroJet strength (IEEJ) and the 6-h average K_p-index prior to the local sunset are the two important parameters, which will give some indication on the state of the background ionospheric conditions around the post-sunset hours. In this paper, the presence of a linear relationship that exists between a function that involves both these parameters (daytime integrated electrojet (IEEJ) strength and the 6-h average K_p-index) and the post-sunset peak height of the F-layer (peak $h'F$) at the equator is presented.

Recent investigations by Basu et al. (1996), Fejer et al. (1999), Anderson et al. (2004) and Tulasi Ram et al. (2006) have consistently shown that there exists a threshold value for the post-sunset vertical drift (PRE $\boldsymbol{E}\times\boldsymbol{B}$ drift) at the equator to favor the occurrence of ESF. Fejer et al. (1999), from Jicamarca radar observations of 200 events during evening and nighttime periods from April 1968 to March 1992, have reported that the threshold drift velocity for the generation of strong early night irregularities varies from 50 m/s during solar maximum to a value of 20 m/s during solar minimum. Tulasi Ram et al. (2006) have shown that the threshold value of this upward $\boldsymbol{E}\times\boldsymbol{B}$ drift at the equator should be $\geq$30 m/s for the onset of strong scintillations over Waltair (17.7° N, 83.3° E) during the high sunspot year 2001, while it reduces to 20 m/s during the low solar activity year, 2004. Devasia et al. (2002), from the ionosonde observations over an Indian equatorial station, Trivandrum during equinoctial periods of March–April 1998, have reported that the ESF appears on ionograms whenever the virtual height of the F-layer ($h'F$) exceeds a threshold value of 300 km, irrespective of the polarity of the meridional winds. Further, Jyoti et al. (2004) have clearly shown that the critical height $(h'F)_c$ of the F-layer for the onset of ESF increases/decreases linearly with solar flux. However, the rationale for this solar activity dependence of the critical/threshold height of the post-sunset F-layer for the onset of ESF still remains unexplained. Here, in this paper, this result is explained, for the first time, on the basis of changes in the local linear growth rate of collisional Rayleigh-Taylor instability due to the variability of various terms, such as the inverse density gradient scale length (L^{-1}), ion-neutral collision frequency (ν_{in}) and recombination rate (R) with the changes in the solar activity.

2 Data and method of analysis

The ionogram data obtained from three identical digital ionospheric sounders operated simultaneously, at an equatorial station Trivandrum (8.47° N, 76.91° E, dip.lat. 0.5° N), an off-equatorial station SHAR (13.7° N, 80.2° E, dip.lat. 10.8° N) and a nearby low latitude station Waltair (17.7° N, 83.3° E, dip.lat. 20° N), during the descending phase of the current solar cycle (2001 to 2005) are considered in the present study. Amplitude scintillations data recorded simultaneously at VHF (244 MHz) from a geostationary satellite FLEETSAT (73° E) over Waltair is also used.

Further, the data from two magnetometers, one situated at the equatorial station (within the ElectroJet region), Tirunelveli (8.7° N, 77.7° E, dip.lat. 0.6° N) and the another at an off-equatorial station (outside the ElectroJet region), Alibagh (18.5° N, 72.9° E, dip.lat. 23.5° N), is used to obtain the variation of the Equatorial ElectroJet (EEJ) strength. The difference between the ΔH values (H-component of the magnetic field after subtracting the night time base level) at Tirunelveli and Alibagh, i.e. ΔH_{T-A} (nT), is taken as a measure of the Equatorial ElectroJet (EEJ) strength (Rusch and Richmond, 1973; Rastogi and Klobuchar, 1990). The details of the various instruments operated at different locations are given in Table 1.

In the present study, we have analyzed the data pertaining only to the equinoctial month of March for the years 2001, 2002, 2004 and 2005 because of the high occurrence probability of ESF in the Indian low-latitude sector during this month. Table 2 shows the number of days considered in this study for each year along with the number of nights with ESF and without ESF occurrence.

The method of calculating the Integrated Equatorial ElectroJet (IEEJ) strength is illustrated in Fig. 2. The Equatorial

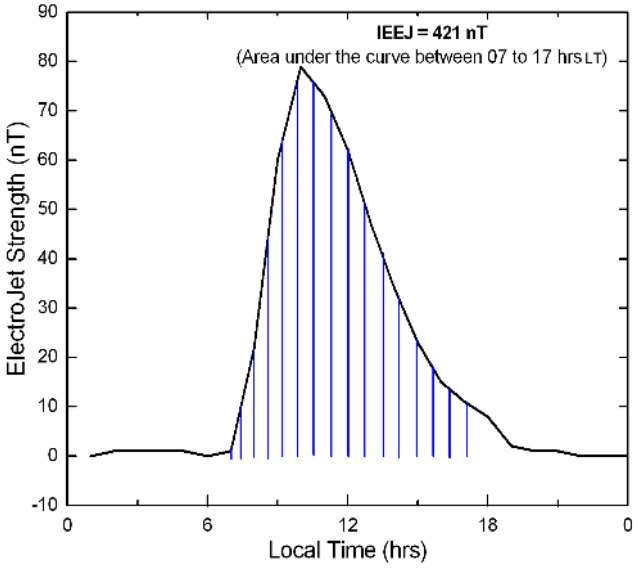

Fig. 2. Method of computing the Integrated Equatorial ElectroJet (IEEJ) strength. The area under the curve measured at each hour between 07:00 and 17:00 LT is taken as IEEJ strength.

ElectroJet (EEJ) strength and (ΔH_{T-A}) values are plotted against the local time with one hour intervals and the area under the curve from 07:00 h to 17:00 h local time (shaded portion) is considered as the IEEJ strength of that day.

The virtual height of the 4-MHz return signal ($h'F$) on the ionograms of the equatorial station, Trivandrum, is taken as the base height of the F-layer, since the difference between the true height and virtual height is very small at this low frequency. The $h'F$ is scaled at every 15-min interval from 18:00 LT (local sunset time) to the onset time of spread-F on the ionograms for each day. For those days on which spread-F has not occurred, the $h'F$ values are scaled between 18:00 and 20:00 LT. The maximum of these $h'F$ values is considered as the post-sunset peak height of the F-layer (herein after called as peak $h'F$) for that day. In the majority of the cases (more than 90%) the peak $h'F$ occurred between 19:00–19:30 LT over Trivandrum.

3 Results and discussion

In order to examine the effect of Integrated Equatorial ElectroJet (IEEJ) strength and the average K_p-index on the post-sunset peak height of the equatorial F-layer, the peak $h'F$ for the month of March 2001, as a function of IEEJ, and the 6-h average K_p-index prior to the local sunset are plotted and presented in Figs. 3a and b, respectively.

From Fig. 3a, it is clearly seen that the peak $h'F$ increases with increasing IEEJ and there exists a linear relationship between these two parameters. The least-squares straight line fit gives a relation between IEEJ and the peak $h'F$ as

Table 1. Geographical locations of the different instruments operated during the period of study.

Station	Geographic co-ordinates		Dip latitude
	Geog. Latitude	Geog. Longitude	
Ionospheric sounders			
Trivandrum	8.47° N	76.91° E	0.5° N
SHAR	13.7° N	80.2° E	10.8° N
Waltair	17.7° N	83.3° E	20° N
Magnetometers			
Tirunelveli	8.7° N	77.7° E	0.6° N
Alibagh	18.5° N	72.9° E	23.5° N
VHF (244 MHz) scintillations			
Waltair	17.7° N	83.3° E	20° N

Table 2. Number of days considered in each year along with number of nights with ESF and without ESF.

Period	Number of days	ESF	No-ESF
March 2001	23	20	3
March 2002	21	19	2
March 2004	26	23	3
March 2005	27	20	7

$$\text{peak } h'F = 366.2 + 0.2 \times \text{IEEJ} \quad (1)$$

with a correlation coefficient, r=0.7.

Further, it is also seen from Fig. 3b that there exists an inverse linear relationship between the 6-h average K_p-index and the peak $h'F$. The least-squares straight line fit equation can be given as

$$\text{peak } h'F = 458.4 - 12.8 \times \text{avg}K_p. \quad (2)$$

The correlation is poor in this case (correlation coefficient r=0.45), as may be seen from the large spread of points on either side of the straight line fit. But the decreasing trend of peak $h'F$ with increasing average K_p-index is clearly evident. Thus, the results shown in Figs. 3a and b clearly suggest that the IEEJ contributes positively for the increase in the post-sunset peak $h'F$, whereas the average K_p-index appears to suppress the post sunset peak height of the F-layer.

The cause and effect relationship between the variations in the IEEJ and the corresponding variations in the height of the equatorial F-layer during the post-sunset hours, as evidenced in the present study, may be explained as follows: it is widely accepted that the post-sunset enhancement of F-region upward drift is basically due to the contribution from the electric fields produced by the F-region dynamo action (Rishbeth, 1971; Farley et al., 1986; Batista et al., 1986; Crain et al., 1993). The main ingredients of F-region dynamo

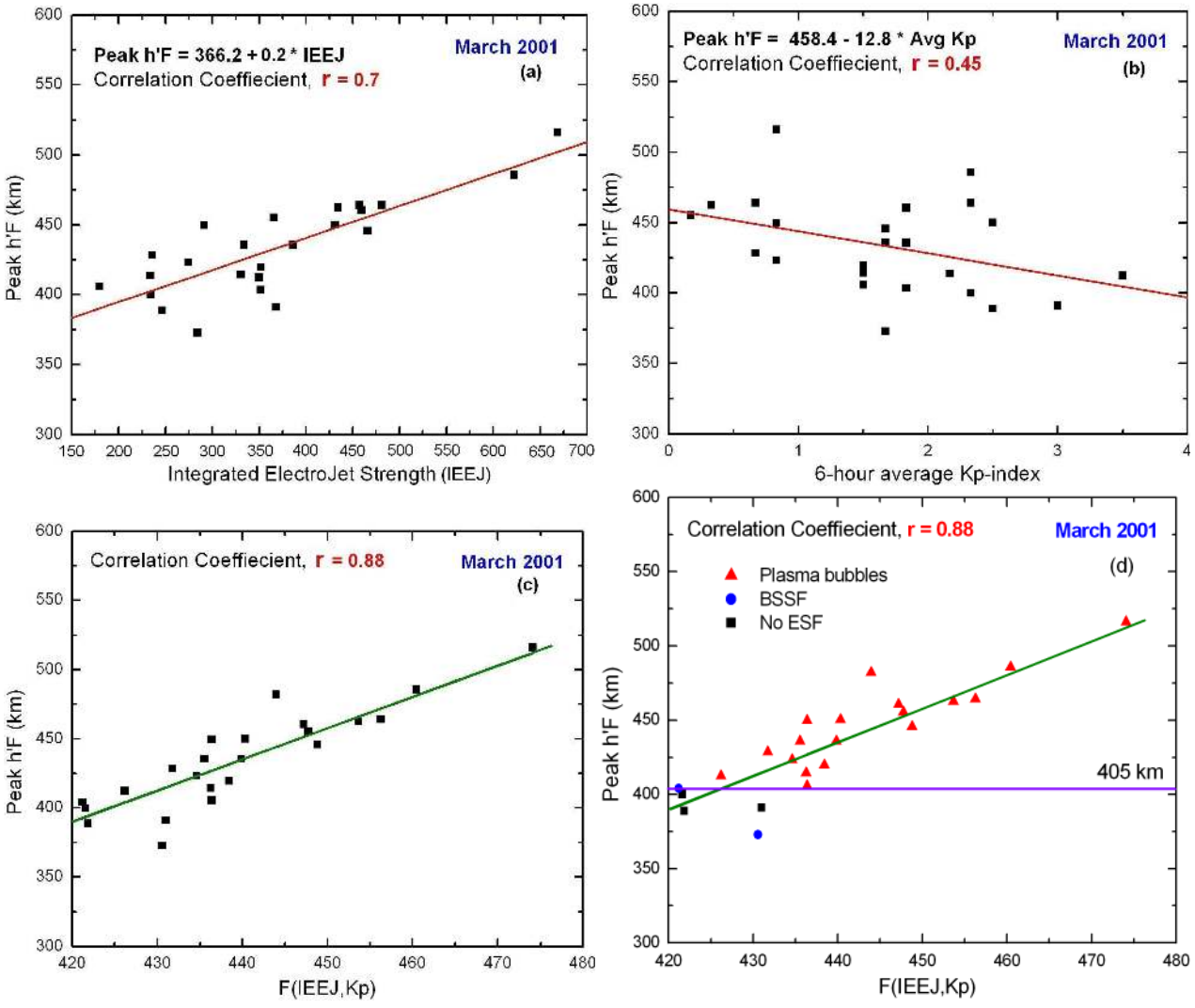

Fig. 3. Plots showing the linear relationship of peak $h'F$ values with IEEJ and average K_p-index **(a)** peak $h'F$ as a function of IEEJ strength, **(b)** peak $h'F$ as a function of 6-h average K_p-index prior to the sunset, **(c)** peak $h'F$ values as a function of the combined parameter F(IEEJ, avg K_p), and **(d)** peak $h'F$ values as a function of the combined parameter F(IEEJ, avg K_p) with color coding (the red triangles representing the peak $h'F$ values for the days on which plasma bubbles were observed, while the blue circles represent the days on which only bottom side spread-F (BSSF) was observed and the black squares represent the days on which no ESF was observed).

action are thermospheric zonal wind ($\boldsymbol{U}$) and the longitudinal gradient in the flux-tube integrated E-region Pederson conductivity across the sunset terminator. The latter depends on the alignment of the sunset terminator with the magnetic meridian, which is not expected to undergo significant day-to-day variations. However, it may vary with season in any given longitudinal sector, leading to the seasonal differences in the post-sunset enhancement of F-layer vertical drifts. In the present study, since we have considered only the equinoctial month of March; the seasonal differences in the post-sunset peak $h'F$ due to flux-tube integrated E-region Pederson conductivity are inconsequential. Hence, the thermospheric zonal wind ($\boldsymbol{U}$) is likely the key factor controlling the F-region dynamo. Also, the zonal wind system at equatorial latitudes can be effectively modulated by the spatial distribution of F-region plasma density (EIA) through ion-neutral drag, which acts as a resistive force for the thermospheric wind dynamics. Large equatorial electrojet strength (which is a consequence of zonal electric field) around the afternoon to pre-sunset hours can effectively operate the fountain process through $\boldsymbol{E}\times\boldsymbol{B}$ drift, thereby intensifying the Equatorial Ionization Anomaly (EIA) during the pre-sunset hours. Also, it has been shown by Raghavarao et al. (1988b), Rama Rao et al. (2006), that there exists a one-to-one correlation between EIA and IEEJ. The intensification of EIA reduces plasma density over the magnetic equator (trough) and

simultaneously increases the plasma density over the ±15–20 dip latitudes (crest regions). The decrease in the plasma density over the equator reduces the ion-drag (which acts as a resistive force) on neutrals and hence enhances the zonal wind ($\boldsymbol{U}$) prior to sunset. Further, the enhanced plasma fountain, in addition, will increase the ratio of F to E-region flux tube integrated Pederson conductivity, due to the increased plasma content along the flux tubes with high apex altitudes over the magnetic equator (Crain et al., 1993). Both of these changes in the properties of the equatorial ionosphere constitute favorable conditions for a very efficient F-region dynamo action, which, in turn, produces a large eastward electric field, thereby causing the large post-sunset height rise of the equatorial F-region.

Fejer et al. (1999), Whalen (2002), Lee at al. (2005) have shown that the extended magnetic activity during equinox solar maximum conditions generally causes large reductions in the amplitude of the post-sunset vertical drifts. Tulasi Ram et al. (2006) have also shown that the pre-reversal enhancements in the $\boldsymbol{E}\times\boldsymbol{B}$ drifts (PRE) decreases linearly with increasing 6-h average K_p-index during both the high (2001) and low (2004) sunspot years. The disturbance dynamo electric fields, which are driven by the enhanced energy deposition into the high-latitude ionosphere during the magnetically disturbed periods, cause a large reduction of the evening upward drifts at the equator, thereby suppressing the post-sunset height rise of the F-layer.

Since the layer height at the post-sunset hours bears a relation with the IEEJ and the average K_p-index, the effects of these two parameters can be combined in the form of a function that involves both IEEJ and average K_p-index. Thus, combining Eqs. (1) and (2), a new equation can be written, as

$$F(\text{IEEJ}, K_p)=\text{peak } h'F=\frac{0.2\times\text{IEEJ}-12.8\times\text{avg}K_p}{2}. \quad (3)$$

Now the peak $h'F$ is plotted against F(IEEJ, K_p) and is presented in Fig. 3c. As may be seen from this figure, the peak $h'F$ holds a good linear relationship with this function and the correlation coefficient is significantly improved (r=0.88). Thus, using this relationship, one can estimate the height of the equatorial F-layer during the post-sunset hours (19:00–19:30 LT) using the IEEJ strength and the 6-h average K_p-index by 17:00 LT with reasonable accuracy.

Figure 3d is similar to that of Fig. 3c, except that the data points are color coded, with red triangles representing the peak $h'F$ values for the days on which plasma bubbles were observed, while the blue circles represent the days on which only bottom side spread-F (BSSF) was observed and the black squares represent the days on which no ESF was observed. In the present study, the presence of plasma bubbles are designated to be on those days when the spread-F is present simultaneously at all stations: Trivandrum (dip. lat. 0.5° N), SHAR (dip. lat. 10.8° N) and Waltair (dip. lat. 20° N) and also the VHF scintillations over Waltair. Those days on which spread-F was observed only at the equatorial stations of Trivandrum and/or SHAR without any ESF over Waltair were designated as BSSF. Further, the high probability of a plasma bubble occurrence during the high solar activity period of March 2001 can be clearly seen from Fig. 3d. It may also be observed from this figure, that the plasma bubbles were observed when the base height of the post-sunset equatorial F-layer is sufficiently high and also there exists a threshold height of 405 km for the development of plasma bubbles during this high solar activity period, March 2001. Here, the threshold height is defined as the minimum height at which the plasma bubble event is observed during that month.

In order to examine the solar activity dependence on the threshold height of the F-layer, similar analyses are also made for the month of March during the years 2002, 2004 and 2005. The variation of the peak $h'F$ values (color coded) against the combined function defined earlier, F(IEEJ, K_p), were plotted for March 2002, 2004 and 2005 and are presented in Figs. 4a, b and c, respectively. As may be seen from these figures, the peak $h'F$ values hold a good linear relationship with the combined function that involves both IEEJ and the average K_p-index during both high (March 2001, 2002) as well as low (March 2004, 2005) solar activity periods. However, the threshold heights for the development of plasma bubbles are found to decrease with decreasing solar activity from the years 2001 to 2005. In Fig. 4d, the variation in the threshold heights of the F-layer as a function of the monthly mean sunspot (mean Rz) number for the months of March 2001, 2002, 2004 and 2005 is presented. The decreasing trend of the threshold height with decreasing solar activity is clearly evident from this figure.

Using the ionogram data of an equatorial station, Trivandrum, during the years from 1993 to 1998, Jyoti et al. (2004) have also reported that the threshold height $(h'F)_c$ for the onset of bottom side spread-F (BSSF), irrespective of the polarity of meridional wind, follows a linear relationship with the solar activity. However, the basis for this solar activity dependence on the threshold height has not been explained.

With a view to investigate the rationale behind the effect of the solar activity on the threshold height, we have examined the effects of different parameters on the local linear growth rate (γ) of the collisional Rayleigh-Taylor instability. Following the method suggested by Lee (2006), the linear growth rate of the CR-T instability is estimated by the equation given by Ossakow et al. (1979), as

$$\gamma = \frac{1}{n_o}.\frac{dn}{dh}.\frac{g}{\nu_{in}} - Rs^{-1}, \quad (4)$$

where n_o is the background electron density, h is the altitude, ν_{in} is the ion-neutral collision frequency, g is the gravity (positive downward), and R is the local recombination rate. The term $(1/n_o)$ (dn/dh) is called the inverse density gradient scale length (L^{-1}) of the background electron density profile. The values of $L^{-1}=(1/n_o)(dn/dh)$ in Eq. (4) are

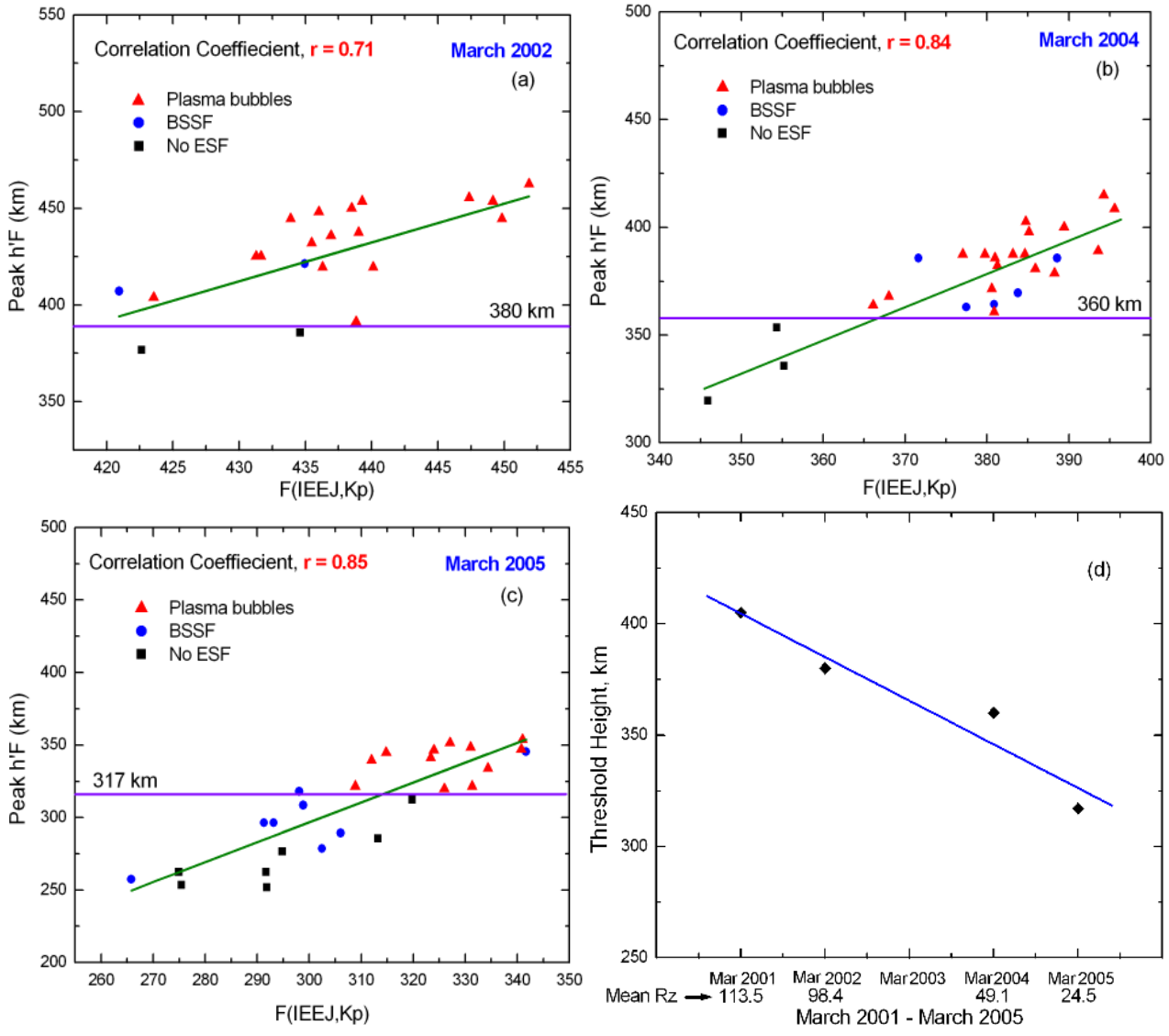

Fig. 4. Plots showing the linear relationship that exists between the post-sunset peak height of the F-layer (peak $h'F$) and the combined function F(IEEJ, avg K_p) that involves both the Integrated ElectroJet strength and the average K_p-Index during the months of **(a)** March 2002, **(b)** March 2004 and **(c)** March 2005, while panel **(d)** presents the variation of the threshold heights as a function of the monthly mean sunspot (mean Rz) number, that are needed for the generation of plasma bubbles.

calculated from the electron density profile over Trivandrum, derived from IRI 2001 model by giving the inputs of sunspot number, *fo*F2 and *hm*F2 values obtained from the ionogram data of Trivandrum.

The ion-neutral collision frequency (ν_{in}) and the recombination rate (R) in Eq. (4) are given by Strobel and McElroy (1970) as

$$\nu_{in} = 2.4 \times 10^{-11} T^{0.5} n_n, s^{-1}, \quad (5)$$

where T is the atmospheric temperature in degrees Kelvin, n_n is the neutral number density in cm^{-3}, and

$$R = K_1 n(O_2) + K_2 n(N_2), \ s^{-1}. \quad (6)$$

In Eq. (6), $n(O_2)$ and $n(N_2)$ are the neutral number densities of O_2 and N_2 in cm^{-3}. The coefficients K_1 and K_2 in Eq. (6) are given (McFarland et al., 1973) as

$$K_1 = 2 \times 10^{-11} \left(\frac{300}{T}\right)^{0.4}, \quad (7)$$

$$K_2 = 1.2 \times 10^{-12} \left(\frac{300}{T}\right) \text{ as } T \leq 750°\text{K}, \quad (8)$$

$$K_2 = 8 \times 10^{-14} \left(\frac{T}{300}\right)^2 \text{ as } T > 750°\text{K}. \quad (9)$$

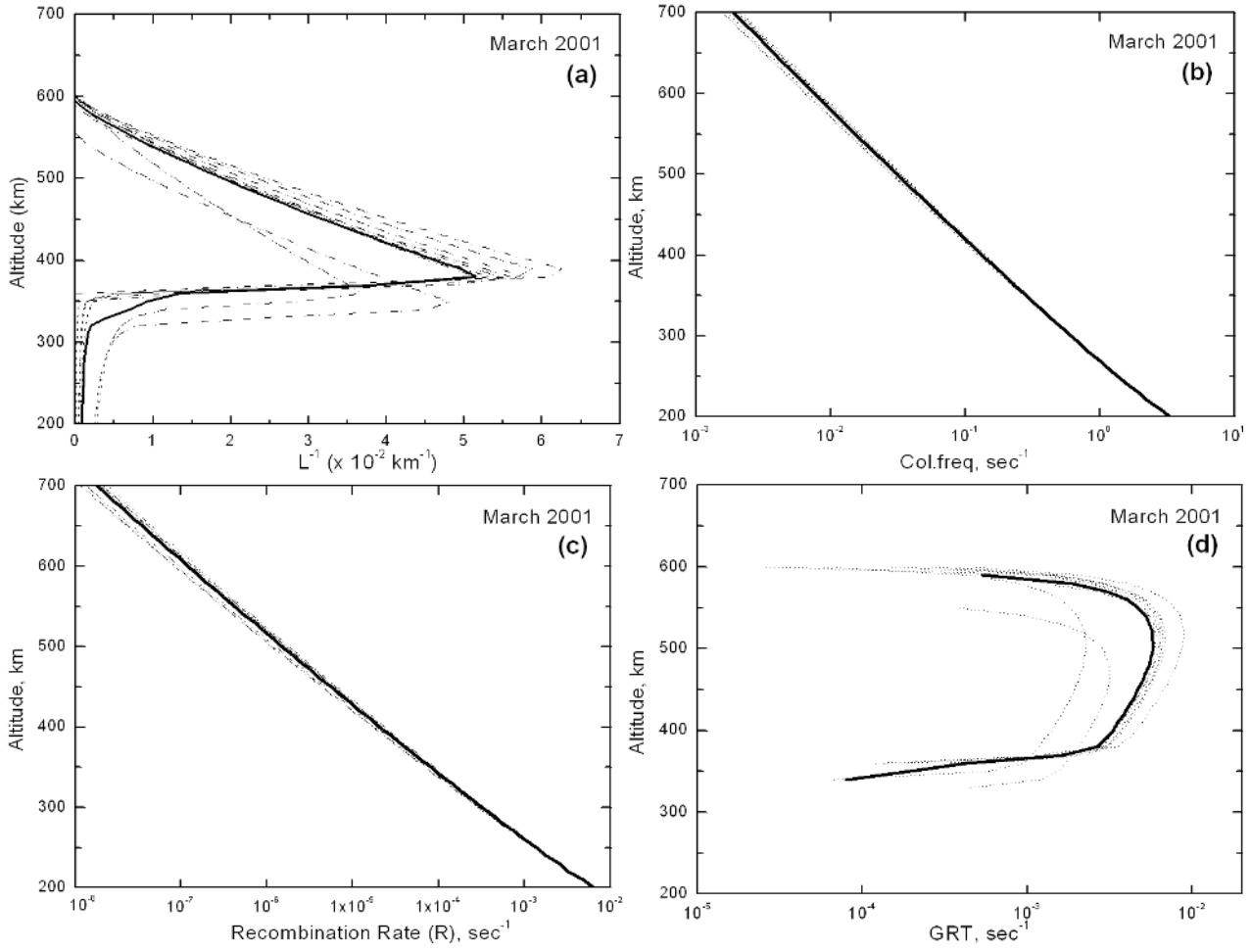

Fig. 5. Altitudinal profiles of **(a)** inverse density gradient scale length (L^{-1}), **(b)** ion-neutral collision frequency (ν_{in}), **(c)** recombination rate (R) and **(d)** the linear growth rate of CR-T instability (γ) at 19:00 LT over Trivandrum during the month of March 2001. The dotted lines are the altitudinal profiles of each day in the month and the solid line represents the monthly mean altitudinal profile for the month of March 2001.

The various atmospheric quantities used in Eqs. (5) through (9) are obtained from the MSISE-90 model (Hedin, 1991).

For example, the computed altitudinal profiles of the inverse density gradient scale length (L^{-1}), ion-neutral collision frequency (ν_{in}), recombination rate (R) and the linear growth rate of the CR-T instability (γ) at 19:00 LT over Trivandrum during the month of March 2001 are presented in Figs. 5a, b, c and d, respectively. In these figures, the dotted lines are the altitudinal profiles at 19:00 LT of each day, whereas the solid line is the monthly mean altitudinal profile for March 2001. As may be seen from Fig. 5d, the linear growth rate of the CR-T instability increases exponentially with increasing altitude due to a decrease in the ion-neutral collision frequency at higher altitudes (Fig. 5b). After reaching a maximum value around 520–530 km, the growth rate (γ) tends to decrease due to the relative contribution from the decreasing L^{-1} with increasing altitude.

Further, in order to examine the variability of L^{-1}, ν_{in}, R and γ with changes in the solar activity, the monthly mean altitudinal profiles for the months of March 2001, 2002, 2004 and 2005 are computed and presented in Fig. 6 as (a), (b), (c) and (d), respectively. It is seen from Fig. 6a that the altitudinal profiles of the inverse density gradient scale length (L^{-1}) during the equinox month (March) of four years closely follow each other between the altitudes of 360 and 380 km. However, between the altitudes of 380 and 500 km, the L^{-1} profiles exhibit a lower value during March 2001 and increases with decreasing solar activity, reaching a maximum during March 2005.

From Figs. 6b and c, it is observed that at any given altitude, both the ion-neutral collision frequency (ν_{in}) and the recombination rate (R) are higher during high solar activity periods and decreases with decreasing solar activity from March 2001 to March 2005. In Fig. 6d, the altitudinal

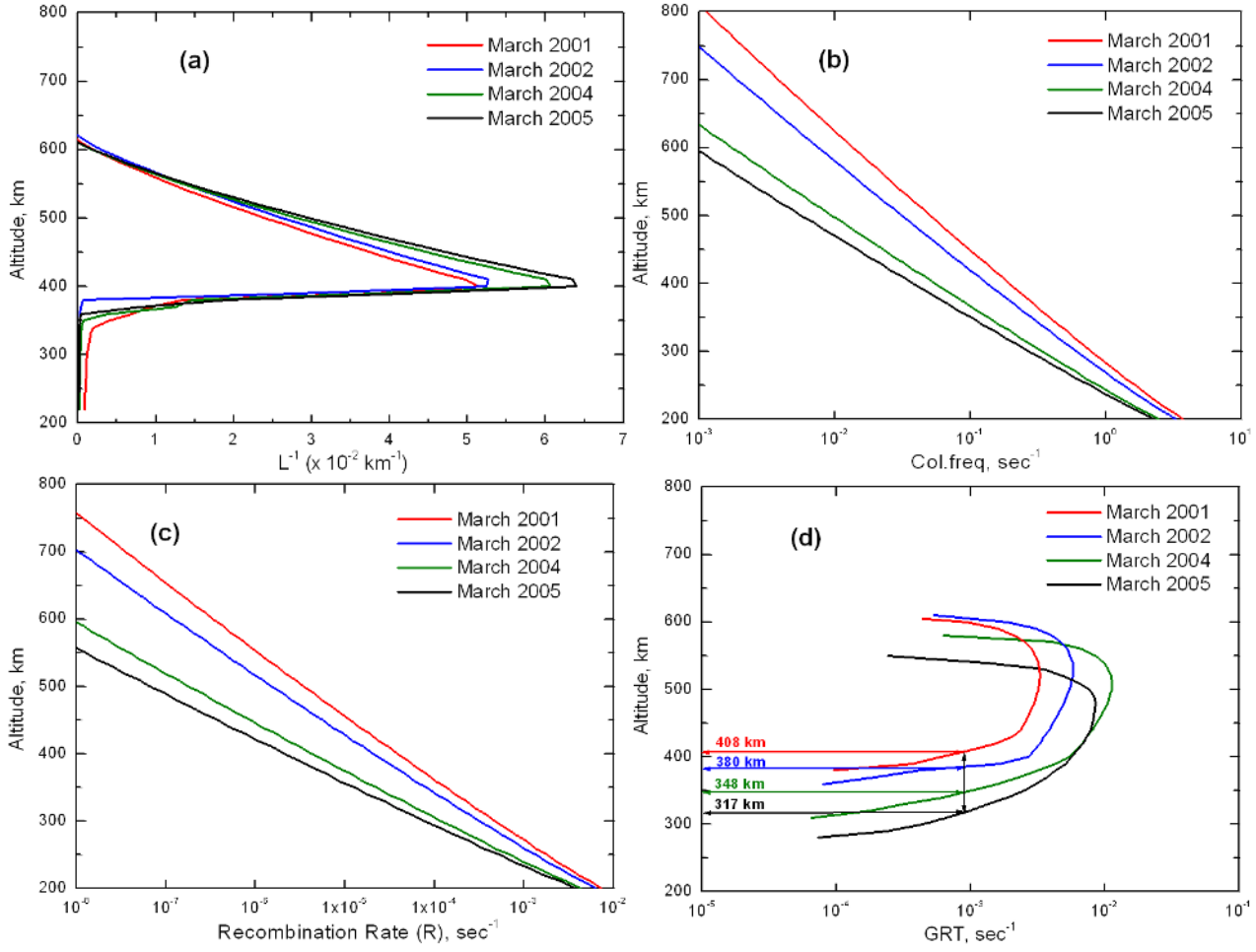

Fig. 6. Monthly mean altitudinal profiles of **(a)** inverse density gradient scale length, L^{-1}, **(b)** ion-neutral collision frequency, ν_{in}, **(c)** recombination rate, R, and **(d)** the local linear growth rate of collisional Rayleigh-Taylor instability γ for the months of March 2001 (red), 2002 (blue), 2004 (green) and 2005 (black).

profiles of linear growth rate of collisional Rayleigh-Taylor (γ) instability for the months of March 2001, 2002, 2004 and 2005 are presented. It is seen from this figure that the growth rate (γ) increases exponentially with altitude (up to the altitudes of about 500–550 km) during all four of these periods. However, for any given growth rate (γ), the corresponding altitudes are lower during the low solar activity periods and higher during the high solar activity periods. For example, from Figs. 4c and d, it may be recalled that the threshold height for a plasma bubble event to occur during the low solar activity period of March 2005 is 317 km. From Fig. 6d, if we consider the growth rate at 317 km during March 2005 as the required growth rate for the development of the plasma bubbles, the same growth rate is obtained at an altitude of 348 km during March 2004, at 380 km during March 2002 and at 408 km during March 2001. In other words, the altitudes at which the necessary growth rate exists for the development of a plasma bubble are 408 km, 380 km, 348 km and 317 km during the periods March 2001, 2002, 2004 and 2005, respectively. Hence, it is inferred from the present study that the altitude at which the necessary growth rate occurs for a plasma bubble to develop decreases linearly with the decreasing solar activity. Also, these values are in good agreement with the measured threshold height values of 405 km, 380 km, 360 km and 317 km, respectively, obtained during the periods March 2001, 2002, 2004 and 2005, as seen in Fig. 4d. Thus, the linear increase/decrease in the threshold post-sunset peak height (peak $h'F$) for the development of plasma bubbles may be explained on the basis of the necessary growth rate that is attained at low altitudes during the low solar activity periods and this altitude increases linearly with the increase in solar activity.

4 Summary

The daytime integrated equatorial electrojet (IEEJ) and the 6-h average K_p-index prior to sunset are the two important parameters that will give some indication of the state of the background ionospheric conditions around the post sunset hours. The IEEJ contributes positively for the post-sunset height rise of the equatorial F-layer, while the disturbed geomagnetic activity (as measured by the average K_p-index) acts as a suppressant. Combining the effects of these two parameters, the combined function, F(IEEJ, avg K_p), is found to bear a linear relationship with the post-sunset peak height (peak $h'F$) of the F-layer. Thus, using this combined function, one can estimate the height of the equatorial F-layer around the post-sunset hours (19:00–19:30 LT) in advance by 17:00 LT with reasonable accuracy and thereby the occurrence of ESF.

Further, the threshold value of the post-sunset F-layer altitude favorable for the development of plasma bubble irregularities is high (405 km) during the high solar activity period of March 2001 (mean Rz=113.5) and decreases linearly with the solar activity to a low value of 317 km during the low solar activity period of March 2005 (mean Rz=24.5). This decrease in the threshold height with the decreasing solar activity is explained as due to the necessary growth rate that is attained at high altitudes during the high solar activity periods and at low altitudes during the low solar activity periods.

The concept of the combined function that can estimate the height of the post-sunset F-layer along with the threshold height and its solar activity variability is very useful in light of forecasting the occurrence of ESF for trans-ionospheric communication and navigational systems. However, the sudden geomagnetic disturbances, which can effectively modulate the equatorial and low-latitude ionosphere within the short time scales of about 2 to 3 h, are still need to be considered. Also, it is expected that the threshold height, as well as the linear relationship between the combined function and the peak $h'F$ could be different during different seasons. Thus, a much larger database is needed to be observed to ascertain the dependence of the combined function and the threshold height on various prevailing ionospheric conditions.

Acknowledgements. This work has been carried out under the Department of Science and Technology (DST), Govt. of India sponsored Project No. SR/S4/AS: 226/03. One of the authors (S. Tulasi Ram) wishes to express his sincere thanks to CSIR, Govt. of India for providing him with a Senior Research Fellowship to carryout this research work. The authors also express their sincere thanks to S. Alex of Indian Institute of Geomagnetism (IIG), N. Mumbai for providing EEJ Strength data.

Topical Editor M. Pinnock thanks E. R. de Paula and another anonymous referee for their help in evaluating this paper.

References

Aarons, J.: The longitudinal morphology of equatorial F layer irregularities relevant to their occurrence, Space Sci. Rev., 63, 209–243, 1993.

Abdu, M. A., Bittencourt, J. A., and Batista, I. S.: Magnetic declination control of the equatorial F region dynamo electric field development and spread F, J.Geophys. Res., 86, 11 443–11 446, 1981.

Anderson, D. N., Reinisch, B., Valladares, C., Chau, J., and Veliz, O.: Forecasting the occurrence of ionospheric scintillation activity in the equatorial ionosphere on a day-to-day basis, J. Atmos. Terr. Phys., 66, 1567–1572, 2004.

Argo, P. E. and Kelley, M. C.: Digital ioinosonde observations during equatorial spread F, J. Geophys. Res., 91, 5539–5555, 1986.

Balsley, B. B., Haerendel, G., and Greenwald, R. A.: Equatorial spread F: Recent observations and a new interpretation, J.Geophys. Res., 77, 5625–5828, 1972.

Basu, S., Kudeki, E., Bsau, Su., et al.: Scintillations, Plasma drifts,and neutral winds in the equatorial ionosphere after sunset, J.Geophys. Res., 101, 26 795–26 809, 1996.

Batista, I. S., Abdu, M. A., and Bittencourt, J. A.: Equatorial F region vertical drift: Seasonal and longitudinal asymmetries in the American Sector, J. Geophys. Res., 91, 12 055–12 064, 1986.

Becker-Guedes, F., Sahai, Y., Fagundes, P. R., Lima, W. L. C., Pillat, V. G., Abalde, J. R., and Bittencourt, J. A.: Geomagnetic storm and equatorial spread-F, Ann. Geophys., 22, 3231–3239, 2004,
http://www.ann-geophys.net/22/3231/2004/.

Booker, H. and Wells, H. W.: Scattering of radio waves in the F region of the ionosphere, J. Geophys. Res., 43, 249–256, 1938.

Chandra, H. and Rastogi, R. G.: Equatorial spread F over a solar cycle, Ann. Geophys., 28, 709–716, 1972,
http://www.ann-geophys.net/28/709/1972/.

Crain, D. J., Heelis, R. A., and Bailey, G. J.: Effects of electrical coupling on equatorial ionosphere plasma motions: When is the F region a dominant driver in the low-latitude dynamics?, J. Geophys. Res., 98, 6033–6037, 1993.

Das Gupta, A., Santimay Basu, Aarons, J., Klobuchar, J. A., Sunanda Basu, and Bushby, A.: VHF amplitude scintillations and associated electron content depletions as observed at Arequipa, Peru, J. Atmos. Terr. Phys., 45, 15–26, 1983.

Devasia, C. V., Jyoti, N., Viswanathan, K. S., Subbarao, K. S. V., Tiwari, D., and Sridharan, R.: On the plausible linkage of thermospheric meridional winds with equatorial spread F, J. Atmos. Sol. Terr. Phys., 64, 1–12, 2002.

Dungey, J. W.: Convective diffusion in the equatorial F-region, J. Atmos. Terr. Phys., 9, 304–310, 1956.

Farley, D. T., Balsley, B. B., Woodman, R. F., and McClure, J. P.: Equatorial spread F: Implications of VHF radar observations, J. Geophys. Res., 75, 7199–7216, 1970.

Farley, D. T., Bonelli, E., Fejer, B. G., and Larsen, M. F.: The prereversal enhancement of the zonal electric field in the equatorial ionosphere, J. Geophys. Res., 91, 13 723–13 728, 1986.

Fejer, B. G. and Kelley, M. C.: Ionospheric irregularities, Rev. Geophys., 18, 401–450, 1980.

Fejer, B. G., Scherliess, L., and de Paula, E. R.: Effects of the vertical plasma drift velocity on the generation and evolution of equatorial spread F, J. Geophys. Res., 104, 19 859–19 869, 1999.

Haerendel, G.: Theroy of equatorial spread F, report, Max-Planck

Inst. for Phys, and Astrophys., Garching, Germany, 1973.

Hedin, A. E.: Extension of the MSIS thermospheric model into the middle and lower atmosphere, J. Geophys. Res., 96, 1159–1172, 1991.

Hysell, D. L. and Burcham, J.: JULIA radar studies of equatorial spread F, J. Geophys. Res., 103, 29 155–29 167, 1998.

Hysell, D. L.: An overview and synthesis of plasma irregularities in equatorial spread F, J. Atmos. Sol. Terr. Phys., 62, 1037–1056, 2000.

Hysell, D. L. and Burcham, J.: Long term studies of equatorial spread F using the JULIA radar at Jicamarca, J. Atmos. Terr. Phys., 64, 1531–1543, 2002.

Jyoti, N., Devasia, C. V., Sridharan R., and Tiwari, D.: Threshold height $(h'F)_c$ for the meridional wind to play a deterministic role in the bottom side equatorial spread F and its dependence on solar activity, Geophys. Res. Lett., 31, L12809, 1–4, doi:10.1029/2004GL019455, 2004.

Kelley, M. C. and Maruyamma, T.: A diagnostic method of equatorial spread F, 2, The effect of magnetic activity, J. Geophys. Res., 97, 1271–1277, 1992.

Kelley, M. C.: The Earth;s ionosphere, Int. Geophys. Ser., Vol.43, Elsevier, New York, 1989.

Lee, C. C.: Examine the local linear growth rate of collisional Rayleigh-Taylor instability during solar maximum, J. Geophys. Res., 111, A11313, 1–5, doi:10.1029/2006JA011925, 2006.

Lee, C. C., Liu, J. Y., Reinisch, B. W., Chen, W. S., and Chu, F. D.: The effects of the pre-reversal drift, the EIA asymmetry, and magnetic activity on the equatorial spread F during solar maximum, Ann. Geophys., 23, 745–751, 2005, http://www.ann-geophys.net/23/745/2005/.

McFarland, M., Albritton, D. L., Fehsenfeld, F. C., Ferguson, E. E., and Schmeltekopf, A. L.: Flow-drift technique for ion mobility and ion-molecule reaction rate constant measurements, 2, Positive ion reaction of N+, O+, and N2 with O2 and O+ with N2 from thermal to ∼2 eV, J. Chem. Phys., 59, 6620–6628, 1973.

Ossakow, S. L., Zalesak, S. T., and McDonald, B. E.: Nonlinear equatorial spread F: Dependence on altitude of the F peak and bottomside background electron density gradient scale length, J.Geophys. Res., 84, 17–29, 1979.

Raghavarao, R., Nageswararao, M., Sastri, J. H., Vyas, G. D., and Sriramarao, M.: Role of equatorial ionization anomaly in the initiation of equatorial spread F, J. Geophys. Res., 93, 5959–5964, 1988a.

Raghavarao. R., Sridharan, R., Sastri, J. H., Agashe, V. V., Rao, B. C. N., Rao, P. B., Somayajulu, V. V.: The Equatorial Ionosphere, Wits Handbook, 1, 48–92, 1988b.

Rama Rao, P. V. S., Gopi Krishna, S., Niranjan, K., and Prasad, D. S. V. V. D.: Temporal and spatial variations in TEC using simultaneous measurements from Indian GPS network of receivers during the low solar activity period of 2004–2005, Ann. Geophys., 24, 1–4, 2006, http://www.ann-geophys.net/24/1/2006/.

Rama Rao, P. V. S., Jayachandran, P. T., and Sri Ram, P.: Ionospheric irregularities-role of Equatorial Ionization Anomaly, Radio Sci., 32(4), 1551–1556, 1997.

Rastogi, R. G. and Klobuchar J. A.: Ionospheric electron content within the equatorial F2 layer anomaly belt, J. Geophys. Res., 95, 19 045–19 052, 1990.

Rastogi, R. G.: Seasonal and solar cycle variations of equatorial spread F in the American sector, J. Atmos. Terr. Phys., 42, 593–597, 1980.

Rishbeth, H.: The F region dynamo, Planet. Space Sci., 19, 263–267, 1971a.

Rusch, C. M. and Richmond, A. D.: The relationship between the structure of the equatorial anomaly and the strength of the equatorial electrojet, J. Atmos. Terr. Phys., 35, 1171–1180, 1973.

Sastri, J. H., Sasidharan, K., Subrahmanyam, V., and Sriramarao, M.: Seasonal and solar cycle effects in the occurrence of equatorial spread F configuration, Ind. J. Radio. Space. Phys., 8, 135–138, 1979.

Sastri, J. H.: Duration of equatorial spread F, Ann. Geophys., 2, 353–358, 1984, http://www.ann-geophys.net/2/353/1984/.

Sastri, J. H.: On the development of abnormally large post sunset upward drift of equatorial F region under quiet geomagnetic conditions, 103(A3), 3983–3991, 1998.

Sridharan, R., Raju, D. P., Raghavarao, R., and Rama Rao, P. V. S.: Precursor to equatorial spread-F in OI 630.0 nm dayglow, Geophys. Res. Lett., 21, 2797–2800, 1994.

Strobel, D. F. and McElroy, M. B.: The F2-layer at middle latitude, Planet. Space Sci., 18, 1181–1202, 1970.

Sultan, P. J.: Linear theory and modeling of the Rayleigh-Taylor instability leading to the occurrence of equatorial spread F, J. Geophys. Res., 101, 26 875–26 891, 1996.

Thampi, S. V., Ravindran, S., Pant, T. K., Devasia, C. V., Sreelatha, P., and Sridharan, R.: Deterministic prediction of post-sunset ESF based on the strength and asymmetry of EIA from ground based TEC measurements: Preliminary results, Geophys. Res. Lett., 33, L13103, 1–4, doi:10.1029/2006GL026376, 2006.

Tulasi Ram, S., Rama Rao, P. V. S., Niranjan, K., Prasad, D. S. V. V. D., Sridharan, R., Devasia, C. V., and Sudha Ravindhran.: The role of post sunset vertical drifts at the equator in predicting the onset of VHF scintillations during high and low sunspot activity years, Ann. Geophys., 24, 1609–1616, 2006, http://www.ann-geophys.net/24/1609/2006/.

Whalen, J. A.: Equatorial bubbles observed at the north and south anomaly crests: Dependence on season, local time and dip latitude, Radio Sci., 32, 1559–1556, 1997.

Whalen, J. A.: An equatorial bubble: Its evolution observed in relation to bottomside spread F and to the Appelton anomaly, J. Geophys. Res., 105, 5303–5315, 2000.

Whalen, J. A.: Dependence of equatorial bubbles and bottomside spread F on season, magnetic activity, and $\boldsymbol{E}\times\boldsymbol{B}$ drift velocity during solar maximum, J. Geophys. Res., 107(A2), 1024–1033, doi:10.1029/2001JA000039, 2002.

Woodman, R. F. and LaHoz, C.: Radar observations of F region equatorial irregularities, J. Geophys. Res., 81, 5447–5466, 1976.